

Spatial Resolution of Numerical Models of Man and Calculated Specific Absorption Rate Using the FDTD Method: A Study at 64 MHz in a Magnetic Resonance Imaging Coil

Christopher M. Collins, PhD* and Michael B. Smith, PhD

Purpose: To examine how fine a model resolution is necessary for calculation of specific energy absorption rate (SAR) for the human head in regions as small as 1 g.

Materials and Methods: Here we perform a simple study comparing the maximum SAR averaged over any 1 cm³ and SAR averaged over the entire head for several models of the same human head within the same radiofrequency coil, but with spatial resolutions varying from 8–100 Yee cells per cm³.

Results: Over the range of model resolutions from 8–100 Yee cells per cm³, there is only a 16% variation in maximum SAR in any 1 cm³ of tissue in the head, and only a 7% variation in SAR averaged over the entire head.

Conclusion: While it is always desirable to perform SAR calculations with the greatest possible accuracy, in calculations of the maximum SAR levels in any 1 cm³ of tissue, spatial resolutions greater than 5 mm may not yield notably different results than those with a spatial resolution of 5 mm.

Key Words: MRI; SAR; safety; FDTD; resolution; calculations

J. Magn. Reson. Imaging 2003;18:383–388.
© 2003 Wiley-Liss, Inc.

MANY RESEARCHERS HAVE USED numerical models of the human head in order to assess specific energy absorption rate (SAR) levels for magnetic resonance imaging (MRI) (1–7). These previous calculations include assessments of SAR in different types of coils at different field strengths and equations for determining SAR for arbitrary pulse sequences (5–7).

Although it is expected that SAR levels depend on the body geometry of the subject, there are very few anatomically-accurate computer-based models of individual subjects available. In preparation for creating new models of different subjects, it is valuable to determine to what resolution it is necessary to create new models. Too low a resolution will not give accurate information. Because the amount of work and computer resources necessary to acquire anatomically accurate information, segment the information into discrete tissues, and perform numerical calculations increases rapidly with increasing model resolution, it is also desirable to create models at a resolution that is not unnecessarily high.

Today there are regulatory limits on SAR in any 1 g of tissue for MRI. Numerical calculations with the finite difference time domain (FDTD) method for electromagnetics (8,9) can be used as an aid to ensure compliance with such limits on SAR in specific MRI experiments (5–7, 10). It is difficult, however, to judge the accuracy of such calculations in predicting local SAR levels in the human body without accurate experimental techniques to validate numerical results. The rule-of-thumb often used in FDTD calculations for ensuring accuracy is that maximum grid spacing be limited to one-tenth of the smallest wavelength. This rule is valid in theory and in practice for plane waves in free space and as distorted by large, homogeneous objects or highly-conductive surfaces. Local SAR levels in the heterogeneous human body, however, are largely a function of available current paths (5, 11, 12). If these current paths, e.g., a continuous, thin layer of skin tissue, are not modeled accurately, then local SAR levels cannot be accurately calculated.

One method to ensure adequate accuracy in numerical calculations is to perform a calculation at increasing levels of accuracy until it is apparent that the quantity of interest varies little with further increases in accuracy. Here we present FDTD calculations of average and maximum local (1-cm³ region) SAR levels for a human head in a saddle coil at anatomically-accurate grid resolutions from 8 Yee cells (8,9) per cm³ to 100 cells/cm³.

Center for NMR Research, Department of Radiology, The Pennsylvania State University College of Medicine, Hershey, Pennsylvania.

Contract grant sponsor: NIH; Contract grant number: R01EB000454.

*Address reprint requests to: C.M.C., Center for NMR Research, NMR/MRI Building, Department of Radiology H066, The Pennsylvania State University College of Medicine, 500 University Drive, Hershey, PA 17033. E-mail: cmcollins@psu.edu

Received December 11, 2002; Accepted May 14, 2003.

DOI 10.1002/jmri.10359

Published online in Wiley InterScience (www.interscience.wiley.com).

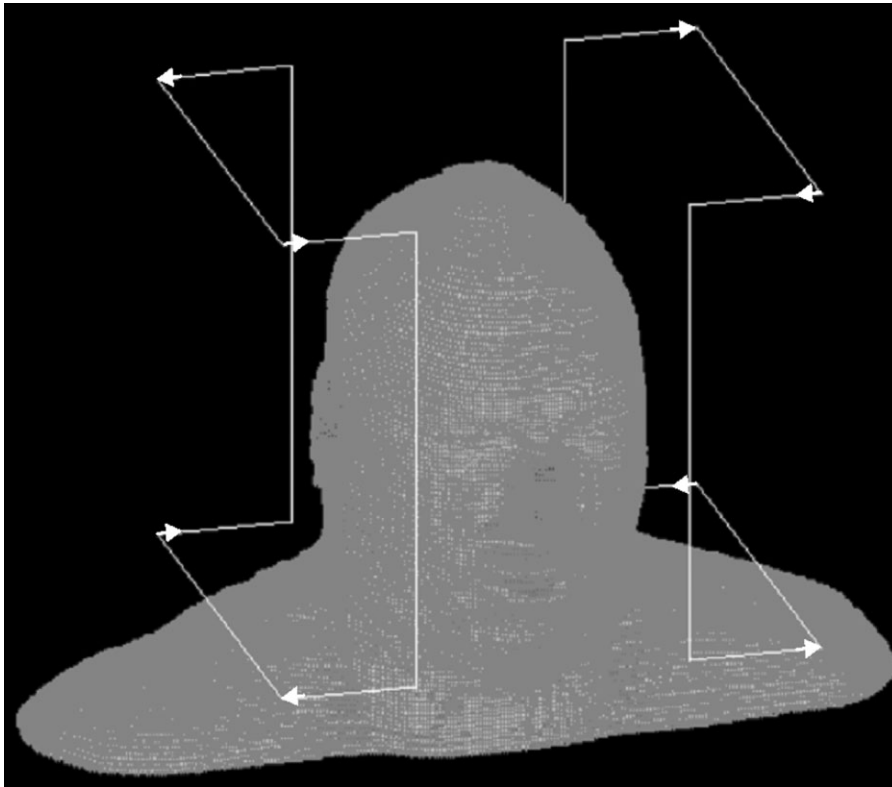


Figure 1. Three-dimensional geometry of head in saddle coil. Arrows indicate position and direction of voltage sources.

MATERIALS AND METHODS

Four models of the human head for use with the FDTD method were created from the color photographic images of the human body in the Visible Male Project of the National Libraries of Medicine (http://www.nlm.nih.gov/research/visible/visible_human.html). The final models have 20 tissues at anatomically-accurate resolutions of 8 cells/cm³ ($\Delta_x, \Delta_y, \Delta_z = 5 \text{ mm}, 5 \text{ mm}, 5 \text{ mm}$), 18 cells/cm³ ($\Delta_x, \Delta_y, \Delta_z = 3.33 \text{ mm}, 3.33 \text{ mm}, 5 \text{ mm}$), 36 cells/cm³ ($\Delta_x, \Delta_y, \Delta_z = 3.33 \text{ mm}, 3.33 \text{ mm}, 2.5 \text{ mm}$), and 100 cells/cm³ ($\Delta_x, \Delta_y, \Delta_z = 2 \text{ mm}, 2 \text{ mm}, 2.5 \text{ mm}$). Here x is in the left-right direction, y is in the anterior-posterior direction, and z is in the superior-inferior direction. Details of the method of model creation have been published previously (6). A three-dimensional representation of the head model in the saddle coil model is given in Figure 1. Sagittal and coronal slices through the highest-resolution model are shown in Figure 2. The tissues in the models

were assigned appropriate electrical parameters for 64 MHz (13).

Identical saddle coils were defined around each of the head models and driven at 64 MHz with voltage sources performing the function of capacitors (Fig. 1). This method of modeling coils with the FDTD method has been proven accurate with experimental verification in a head-sized birdcage coil loaded with water, saline, and the human head up to 128 MHz (14) and in a surface coil loaded with head-sized spheres of saline up to 300 MHz (15). Initially all voltage sources were assigned a magnitude of 1.0 V. The saddle coil was chosen because it could easily be designed and located in such a manner that its shape and location would not vary with model resolution (Fig. 1). Commercially available software ("xfldtd"; Remcom; State College, PA) was used in setting up and solving all FDTD problems.

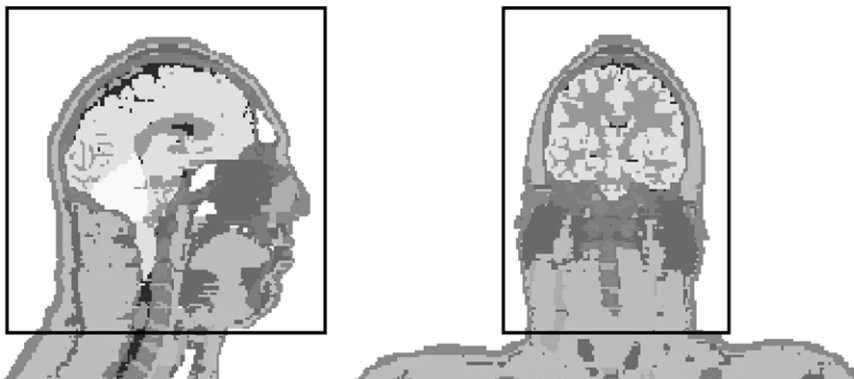


Figure 2. Region considered "head" for evaluation of SAR. Tissues in box-shaped region are considered part of head. Exclusion of shoulders both avoids inaccuracies introduced at inferior boundary of model and allows for comparison with IEC limits for SAR levels in the head.

The calculated electrical and magnetic fields were normalized to produce a radiofrequency magnetic (\mathbf{B}_1) field with a circularly-polarized component (B_1^+) having a magnitude of 1.957 μT (as if to produce a 3 msec, 90° rectangular pulse) at the center of the coil. The resulting field distribution is equivalent to the result that would be obtained by driving with a voltage source magnitude equal to the necessary normalization factor in volts. Then the average SAR over the head region and the maximum SAR averaged over any 1 cm^3 in the head region (within box in Figure 2: excluding shoulders and inferior boundary of model) were calculated from the steady-state FDTD data. All volume average SAR values were calculated as:

$$\text{SAR} = \frac{1}{N} \sum_{n=1}^N \left(\frac{\sigma_{xn} E_{xn}^2}{2\rho_{xn}} + \frac{\sigma_{yn} E_{yn}^2}{2\rho_{yn}} + \frac{\sigma_{zn} E_{zn}^2}{2\rho_{zn}} \right) \quad (1)$$

where the summation is over all N locations in the volume of interest, σ_{xn} , σ_{yn} , and σ_{zn} represent the conductivity of Yee cell elements oriented in the x , y , and z directions at the n th location, E_{xn} , E_{yn} , and E_{zn} represent the peak magnitude of electrical field components oriented in the x , y , and z directions at the n th location, and ρ_{xn} , ρ_{yn} , and ρ_{zn} represent the mass density of Yee cell elements oriented in the x , y , and z directions at the n th location. With this method we assume the SAR in a given cell to be a function of the current densities, electrical fields, and anisotropic tissue properties at a single vertex. Other methods using field values and tissue properties from neighboring vertices to estimate a single SAR value in a cell have been proposed in order to improve theoretical accuracy, but have been shown to produce SAR values similar to those produced with a method like that used here, especially at high resolutions (16). All Yee cell elements assigned properties of air were excluded from the summation.

RESULTS

Shaded plots of the \mathbf{B}_1 field magnitude and SAR distributions in the highest-resolution head model as induced by the saddle coil when driven with 1 V are given in Figure 3. The B_1 field is strongest near the wires and is oriented primarily in the left-right direction of the model within the volume of the coil. SAR is greatest toward the outside of the head along pathways through which the greatest B_1 flux passes, as consistent with Faraday's Law and the availability of electrical current pathways due to the distribution of tissue conductivities. This general SAR distribution would be fairly consistent with that induced by any fairly homogeneous volume coil at 64 MHz with a linear B_1 field oriented in the left-right direction (5), or with the SAR distribution induced by the left-right component of a quadrature coil. SAR distributions on an axial plane and the location of the maximum SAR in any 1-cm^3 region at all mesh resolutions are given in Figure 4. Increasing resolution, from top to bottom of Figure 4, is apparent in SAR distribution (left) and shown in sagittal anatomical

representation of model (right). Table 1 gives the normalization factor (driving voltage) necessary to produce a \mathbf{B}_1 field with a circularly-polarized component having a magnitude (B_1^+) of 1.957 μT (as if to produce a 3 msec, 90° rectangular pulse) at the center of the coil, and the maximum one-cell, maximum 1 cm^3 , and average SAR levels when the coil is driven with a voltage equal to the normalization factor in volts at each resolution.

DISCUSSION

Models of the human head were created at four different resolutions directly from anatomical data. Because model resolution was increased with anatomical accuracy in this way (rather than merely subdividing Yee cells from a lower-resolution model), the accuracy with which available current paths in the head are represented was also increased. Therefore, the highest-accuracy calculations here are those at 100 cells/cm^3 .

The \mathbf{B}_1 field magnitude and SAR distributions calculated here are particular to the coil, region of the body, and radiofrequency used in these calculations. Distributions in different coils, regions of the body, or at other frequencies are expected to vary widely (5–7). In this case, where the \mathbf{B}_1 field is oriented primarily in the left-right direction within the head and wavelength effects are expected to be minimal, induced current loops will exist primarily in sagittal planes, increasing toward the model surface but also strongly dependent on multi-tissue model geometry. This is consistent with the result in Figure 3, as SAR is a direct result of the induced current.

As grid dimensions decrease, the maximum SAR in any one cell increases (Table 1). Over the range of model resolutions examined in this study, the smaller the cell dimensions, the higher the maximum local SAR level in one cell. This is to be expected, as an increase in resolution allows for better definition of field and current maxima near interfaces between dissimilar materials and in thin conductive structures. The relevance of this increase in single-cell SAR with increasing model resolution is unclear, however, because temperature is seen to vary spatially at a much more gradual rate than SAR (17), and a possible SAR-induced temperature increase may cause unsafe conditions for the subject. The relation between model resolution and calculated temperature increase may warrant future study. As grid dimensions decrease there is also seen to be a small increase in the normalization factor, or driving voltage required to maintain a constant \mathbf{B}_1 field magnitude at the center of the coil (Table 1). This is due to slight changes in the effective total inductance of the conductors and in the size of the voltage gaps. The fact that there is no general upward or downward trend in whole-head average SAR or in maximum 1-cm^3 average SAR (Table 1) indicates that the variation in these values is more an indication of calculation accuracy. We would expect the variation in these values to decrease for calculations performed at a range of increasingly high resolutions, just as the difference in values between the two highest-resolution calculations is less than the difference in values for the two lowest-resolution calcula-

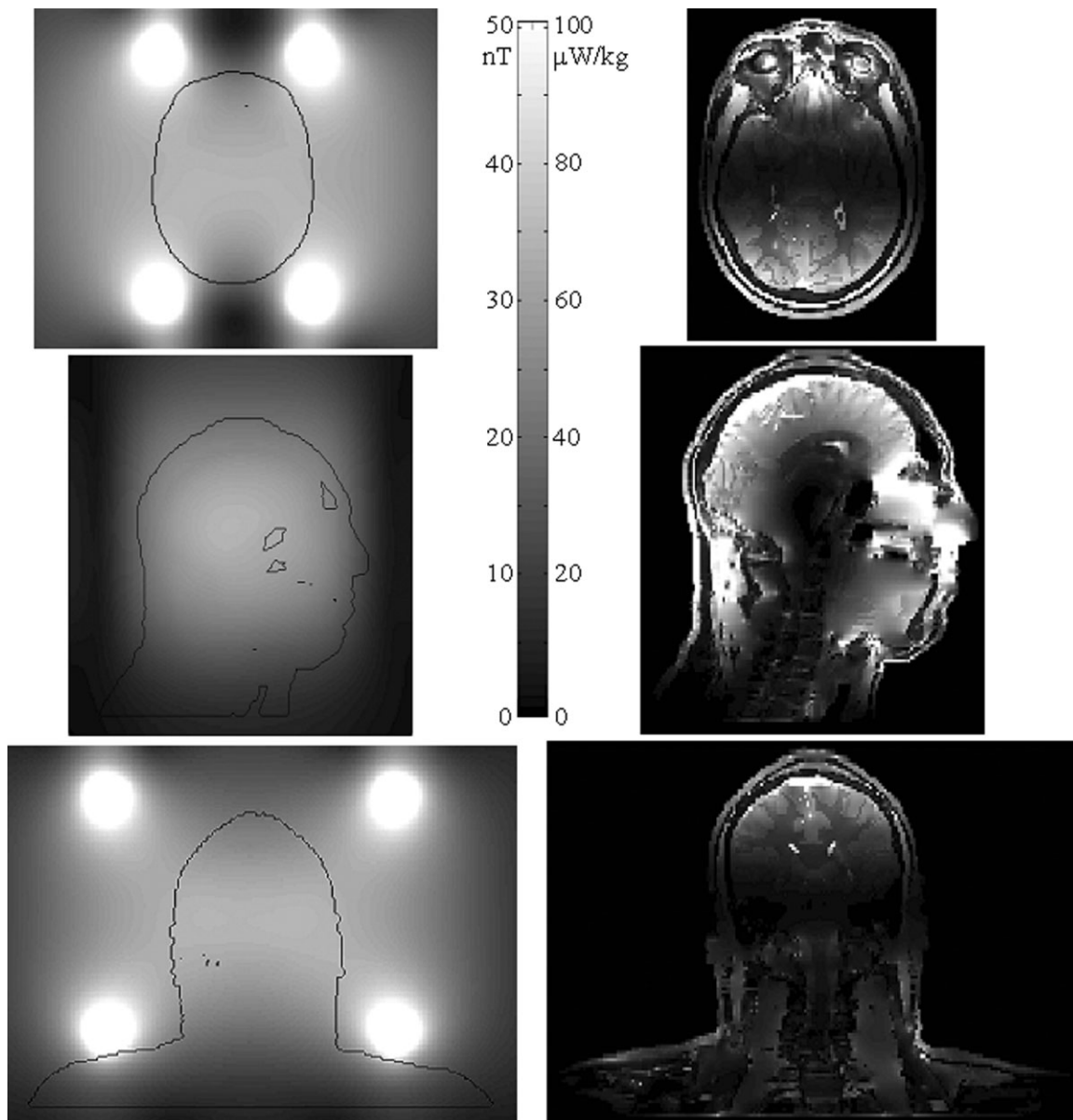


Figure 3. Distribution of $|B_1|$ (left) and SAR (right) for highest-resolution ($\Delta_x, \Delta_y, \Delta_z = 2 \text{ mm}, 2 \text{ mm}, 2.5 \text{ mm}$) head model in saddle coil before normalization (driving voltage = 1 V). Axial (top), sagittal (middle) and coronal (bottom) slices are all through middle of coil. Color bar gives numerical values associated with gray shades. Values above maximum value in scale are represented with the same (white) color.

tions (both shown here) for both the whole-head average SAR and the maximum 1-cm³ average SAR.

The International Electrotechnical Commission (IEC) and the United States Food and Drug Administration (FDA) have defined limits for the maximum SAR a patient can receive during an MRI examination (10,18). The limits are defined for average SAR over the whole body, over the whole head, and in any 1 g of tissue in the head, torso, or extremities. Since maximum conductivities and SAR levels tend to occur in soft tissue (density $\approx 1 \text{ g/cm}^3$) it is appropriate to use the SAR in 1 cm³ to compare to limits in 1 g of tissue. Discussion of how these limits can be related to specific MRI experiments using FDTD calculations has been given elsewhere (5–7). Over a range of mesh resolutions from

8–100 cells/cm³, the maximum 1-cm³ average SAR is seen to vary by only about 16% of the value calculated at 100 cells/cm³ (Table 1) and the location of the maximum 1-cm³ SAR is not seen to change (Fig. 4). Similarly, over a range of mesh resolutions from 8 cells/cm³ to 100 cells/cm³, the whole-head average SAR is seen to vary by only about 7% of the value calculated at 100 cells/cm³ (Table 1).

Considering calculation results at 900 MHz for cellular phones, there may be a greater variation in maximum 1-cm³ average SAR values due to differences in head geometry (19) than seen here due to mesh resolution. Though we have no reason to expect larger differences in SAR values at mesh resolutions much greater than 100 cells/cm³, we cannot rule out

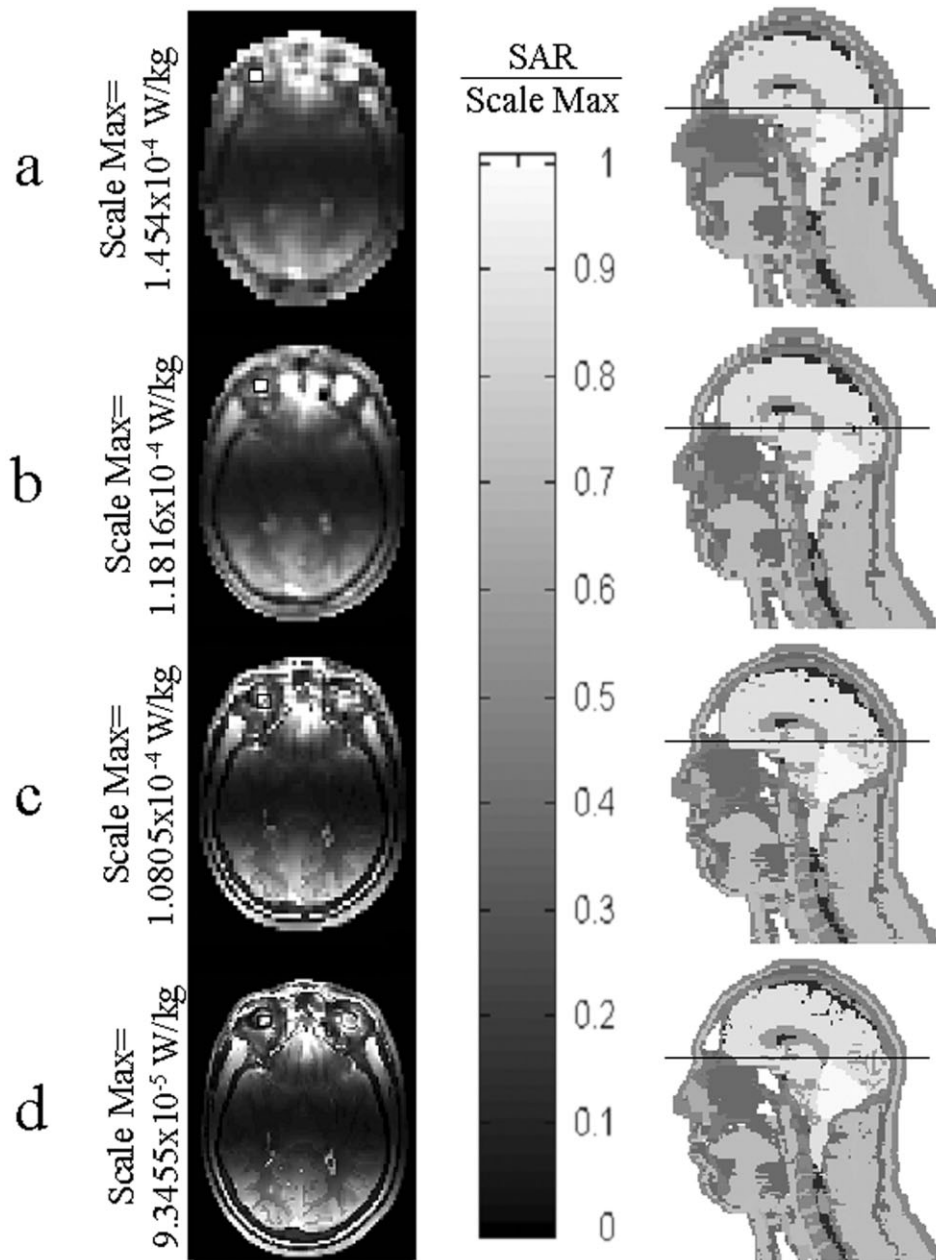


Figure 4. Location of cm^3 with maximum SAR before normalization (driving voltage = 1 V) for head in saddle coil at mesh resolutions of 8 (a), 18 (b), 36 (c), and 100 (d) cells per cm^3 . Line in anatomical sagittal slice (right) shows location of axial SAR distribution plot (left). Axial plane shown is through grid location immediately inferior to center of cm^3 with maximum average SAR. Black square (in eye region on viewer's left) shows location of cm^3 with maximum average SAR for each calculation. SAR values are given in the color bar, with values above the maximum in the scale represented with the same (white) color. Scale maximum at each resolution is three times the mean SAR in the head on the plane shown.

this possibility from this study alone. Still, it appears that SAR values are relatively stable over a range of mesh resolutions from 8 cells/ cm^3 to 100 cells/ cm^3 . While it is always desirable to perform calculations regarding the safety of human subjects to the greatest degree of accuracy possible, it appears from this

study that calculations performed at 100 cells/ cm^3 present no real advantage over those at 8 cells/ cm^3 for comparison to regulatory limits on SAR in 1g of tissue or averaged over the head. This is especially true when considering the effect of different head geometries on SAR levels (19).

Table 1
SAR Values for Head in Saddle Coil at Different Mesh Resolutions

$\Delta_x, \Delta_y, \Delta_z$ (mm); cells per cm^3	Field normalization factor (driving voltage)	Maximum one-cell SAR (w/kg)	Maximum one- cm^3 SAR (w/kg)	Whole-head average SAR (w/kg)
5, 5, 5; 8	143.3	8.597	6.693	0.8876
$3\frac{1}{3}, 3\frac{1}{3}, 5; 18$	162.1	16.91	7.996	0.9501
$3\frac{1}{3}, 3\frac{1}{3}, 2.5; 36$	162.6	23.16	7.421	0.9285
2, 2, 2.5; 100	175.1	37.96	6.840	0.9342

In conclusion, as computational resources become more powerful and more accessible it will always be possible to perform calculations at higher spatial resolution, but it is currently very tedious to produce high-resolution multi-tissue models of the human body. Here we have attempted to examine what resolution is necessary for adequate evaluation of safety. Our results indicate that a calculation performed with a resolution of 100 cells per cm^3 will not yield notably different results than a calculation performed with a resolution of 8 cells per cm^3 in calculations of local (1 cm^3) and average SAR for a human head in a volume imaging coil at 64 MHz.

REFERENCES

1. Grandolfo M, Vecchia P, Gandhi OP. Magnetic resonance imaging: calculation of rates of energy absorption by a human-torso model. *Bioelectromagnetics* 1990;11:117-128.
2. Simunic D, Wach P, Renhart W, Stollberger R. Spatial distribution of high-frequency electromagnetic energy in human head during MRI: numerical results and measurements. *IEEE Trans Biomed Eng* 1996;43:88-94.
3. Jin J, Chen J. On the SAR and field inhomogeneity of birdcage coils loaded with the human head. *Magn Reson Med* 1997;38:953-963.
4. Ibrahim TS, Lee R, Baertlein BA, Robitaille PML. B1 field homogeneity and SAR calculations for the birdcage coil. *Phys Med Biol* 2001;46:609-619.
5. Collins CM, Li S, Smith MB. SAR and B1 field distributions in a heterogeneous human head model within a birdcage coil. *Magn Reson Med* 1998;40:847-856.
6. Collins CM, Smith MB. Signal-to-noise ratio and absorbed power as functions of main magnetic field strength and definition of "90°" RF pulse for the head in the birdcage coil. *Magn Reson Med* 2001;45:684-691.
7. Collins CM, Smith MB. Calculations of B₁ distribution, SNR, and SAR for a surface coil against an anatomically-accurate human body model. *Magn Reson Med* 2001;45:692-699.
8. Yee KS. Numerical solution of initial boundary value problems involving Maxwell's equations in isotropic media. *IEEE Trans Antennas Propagat* 1966;14:302-307.
9. Kunz KS, Luebbers RJ. The finite difference time domain method for electromagnetics. Boca Raton: CRC Press; 1993. 448 p.
10. International Electrotechnical Commission. Medical electrical equipment - part 2: particular requirements for the safety of magnetic resonance equipment for medical diagnosis, 2nd revision. IEC 601-2-33. 2002.
11. Knopp MV, Essig M, Jurgen D, Zabel H-J, van Kaick G. Unusual burns of the lower extremities caused by a closed conducting loop in a patient at MR imaging. *Radiology* 1996;200:572-575.
12. Davis PL, Shang C, Talagala L, Pasculle WA. Magnetic resonance imaging can cause focal heating in a nonuniform phantom. *IEEE Trans Biomed Eng* 1993;40:1324-1327.
13. Gabriel C. Compilation of the dielectric properties of body tissues at RF and microwave frequencies. Brooks Air Force Base, Texas: Air Force Materiel Command. AL/OE-TR-1996-0037, 1996.
14. Alecci M, Collins CM, Smith MB, Jezzard P. Radio frequency magnetic field mapping of a 3 Tesla birdcage coil: experimental and theoretical dependence on sample properties. *Magn Reson Med* 2002;46:379-385.
15. Collins CM, Yang QX, Wang JH, et al. Different excitation and reception distributions with a single-loop transmit-receive surface coil near a head-sized spherical phantom at 300 MHz. *Magn Reson Med* 2002;47:1026-1028.
16. Caputa K, Okoniewski M, Stuchly MA. An algorithm for computations of the power deposition in human tissue. *IEEE Antennas and Propagation Magazine* 1999;41:102-107.
17. Collins CM, Liu W, Wang J, Smith MB. Temperature calculations for a multi-tissue human head within volume and surface coils at 64 and 300 MHz. In: *Proceedings of the 10th Annual Meeting of ISMRM, Honolulu, 2002*, p. 704.
18. United States Food and Drug Administration. Magnetic resonance diagnostic device; panel recommendation and report on petitions for MR reclassification. *Federal Register* 1988;53:7575-7579.
19. Schonborn F, Burkhardt M, Kuster N. Differences in energy absorption between heads of adults and children in the near field of sources. *Health Phys* 1998;74:160-168.